nature astronomy

SUPPLEMENTARY INFORMATION

https://doi.org/10.1038/s41550-019-1007-5

In the format provided by the authors and unedited.

The violent collisional history of aqueously evolved (2) Pallas

Michaël Marsset[1,2*], Miroslav Brož[3], Pierre Vernazza[4], Alexis Drouard[4], Julie Castillo-Rogez[5], Josef Hanuš[3], Matti Viikinkoski[6], Nicolas Rambaux[7], Benoît Carry[8], Laurent Jorda[4], Pavel Ševeček[3], Mirel Birlan[7,9], Franck Marchis[10], Edyta Podlewska-Gaca[11,12], Erik Asphaug[13], Przemyslaw Bartczak[11], Jérôme Berthier[7], Fabrice Cipriani[14], François Colas[7], Grzegorz Dudziński[11], Christophe Dumas[15], Josef Ďurech[3], Marin Ferrais[4,16], Romain Fétick[4], Thierry Fusco[4,17], Emmanuel Jehin[16], Mikko Kaasalainen[6], Agnieszka Kryszczynska[11], Philippe Lamy[4], Hervé Le Coroller[4], Anna Marciniak[11], Tadeusz Michalowski[11], Patrick Michel[8], Derek C. Richardson[18], Toni Santana-Ros[19,20], Paolo Tanga[8], Frédéric Vachier[7], Arthur Vigan[4], Olivier Witasse[14] and Bin Yang[21]

[1]Department of Earth, Atmospheric and Planetary Sciences, MIT, Cambridge, MA, USA. [2]Astrophysics Research Centre, Queen's University Belfast, Belfast, UK. [3]Institute of Astronomy, Charles University, Prague, Czech Republic. [4]Aix Marseille Univ, CNRS, CNES, Laboratoire d'Astrophysique de Marseille, Marseille, France. [5]Jet Propulsion Laboratory, California Institute of Technology, Pasadena, CA, USA. [6]Mathematics and Statistics, Tampere University, Tampere, Finland. [7]IMCCE, Observatoire de Paris, Paris, France. [8]Université Côte d'Azur, Observatoire de la Côte d'Azur, CNRS, Laboratoire Lagrange, Nice, France. [9]Astronomical Institute of the Romanian Academy, Bucharest, Romania. [10]SETI Institute, Carl Sagan Center, Mountain View, CA, USA. [11]Astronomical Observatory Institute, Faculty of Physics, Adam Mickiewicz University, Poznań, Poland. [12]Institute of Physics, University of Szczecin, Szczecin, Poland. [13]School of Earth and Space Exploration, Arizona State University, Tempe, AZ, USA. [14]European Space Agency, ESTEC – Scientific Support Office, Noordwijk, The Netherlands. [15]TMT Observatory, Pasadena, CA, USA. [16]Space Sciences, Technologies and Astrophysics Research Institute, Université de Liège, Liège, Belgium. [17]ONERA, The French Aerospace Lab, Châtillon, France. [18]Department of Astronomy, University of Maryland, College Park, MD, USA. [19]Departamento de Física, Ingeniería de Sistemas y Teoría de la Señal, Universidad de Alicante, Alicante, Spain. [20]Institut de Ciències del Cosmos, Universitat de Barcelona (IEEC-UB), Barcelona, Spain. [21]European Southern Observatory (ESO), Santiago, Chile. *e-mail: mmarsset@mit.edu

The violent collisional history of aqueously evolved (2) Pallas

Michaël Marsset[1,2], Miroslav Brož[3], Pierre Vernazza[4], Alexis Drouard[4], Julie Castillo-Rogez[5], Josef Hanuš[3], Matti Viikinkoski[6], Nicolas Rambaux[7], Benoît Carry[8], Laurent Jorda[4], Pavel Ševeček[3], Mirel Birlan[7,9], Franck Marchis[10], Edyta Podlewska-Gaca[11,12], Erik Asphaug[13], Przemyslaw Bartczak[11], Jérôme Berthier[7], Fabrice Cipriani[14], François Colas[7], Grzegorz Dudziński[11], Christophe Dumas[15], Josef Ďurech[3], Marin Ferrais[4,16], Romain Fétick[4], Thierry Fusco[4,17], Emmanuel Jehin[16], Mikko Kaasalainen[6], Agnieszka Kryszczynska[11], Philippe Lamy[4], Hervé Le Coroller[4], Anna Marciniak[11], Tadeusz Michalowski[11], Patrick Michel[8], Derek C. Richardson[18], Toni Santana-Ros[19,20], Paolo Tanga[8], Frédéric Vachier[7], Arthur Vigan[4], Olivier Witasse[14], Bin Yang[21]

[1] *Department of Earth, Atmospheric and Planetary Sciences, MIT, 77 Massachusetts Avenue, Cambridge, MA 02139, USA*

[2] *Astrophysics Research Centre, Queen's University Belfast, Belfast BT7 1NN, United Kingdom*

[3] *Institute of Astronomy, Charles University, Prague, V Holešovičkách 2, CZ-18000, Prague 8, Czech Republic*

[4] *Aix Marseille Univ, CNRS, CNES, Laboratoire d'Astrophysique de Marseille, Marseille, France*

[5] *Jet Propulsion Laboratory, California Institute of Technology, 4800 Oak Grove Drive, Pasadena, CA 91109, USA*

[6] *Mathematics and Statistics, Tampere University, 33720 Tampere, Finland*

[7] *IMCCE, Observatoire de Paris, 77 avenue Denfert-Rochereau, F-75014 Paris Cedex, France*

[8] *Université Côte d'Azur, Observatoire de la Côte d'Azur, CNRS, Laboratoire Lagrange, France*

[9]Astronomical Institute of the Romanian Academy, 5-Cuţitul de Argint 040557 Bucharest, Romania

[10]SETI Institute, Carl Sagan Center, 189 Bernado Avenue, Mountain View CA 94043, USA

[11]Astronomical Observatory Institute, Faculty of Physics, Adam Mickiewicz University, Słoneczna 36, 60-286 Poznań, Poland

[12]Institute of Physics, University of Szczecin, Wielkopolska 15, 70-453 Szczecin, Poland

[13]School of Earth and Space Exploration, Arizona State University, Tempe, AZ 85287, USA

[14]European Space Agency, ESTEC – Scientific Support Office, Keplerlaan 1, Noordwijk 2200 AG, The Netherlands

[15]TMT Observatory, 100 W. Walnut Street, Suite 300, Pasadena, CA 91124, USA

[16]Space sciences, Technologies and Astrophysics Research Institute, Université de Liège, Allée du 6 Août 17, 4000 Liège, Belgium

[17]ONERA, The French Aerospace Lab BP72, 29 avenue de la Division Leclerc, 92322 Chatillon Cedex, France

[18]Department of Astronomy, University of Maryland, College Park, MD 20742-2421, USA

[19]Departamento de Física, Ingeniería de Sistemas y Teoría de la Señal, Universidad de Alicante, E-03080 Alicante, Spain

[20]Institut de Ciències del Cosmos, Universitat de Barcelona (IEEC-UB), Martí i Franquès 1, E-08028 Barcelona, Spain

[21]European Southern Observatory (ESO), Alonso de Cordova 3107, 1900 Casilla Vitacura, Santiago, Chile

Supplementary material

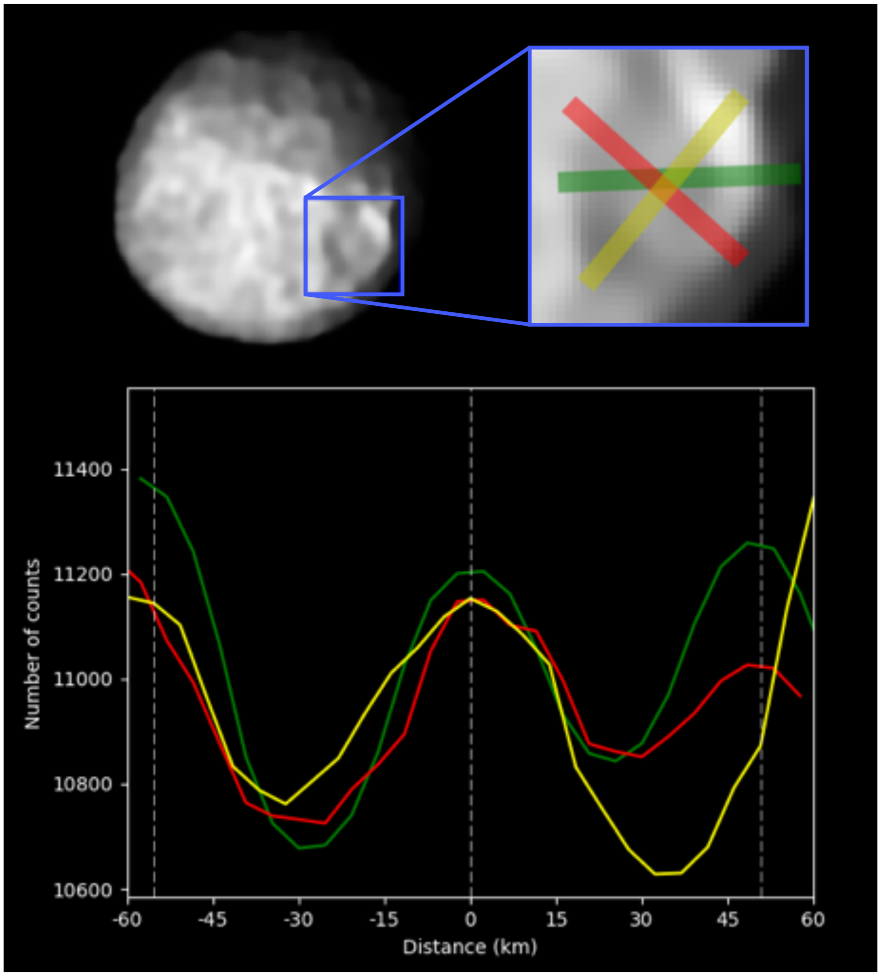

Supplementary Figure 1: **Complex crater with central peak on Pallas.** The top left image shows a view of the southern hemisphere of Pallas, with squared luminosity scale to enhance brightness variations. A zoom on crater Hoplon $((\lambda, \beta) = (230, \text{-}58)^{\circ}$, $D_{\mathrm{c}} \approx 115\,\mathrm{km})$ is shown at the top right. The brightness profile of the crater along the three coloured segments (bottom panel) provides evidence for the presence of a central peak.

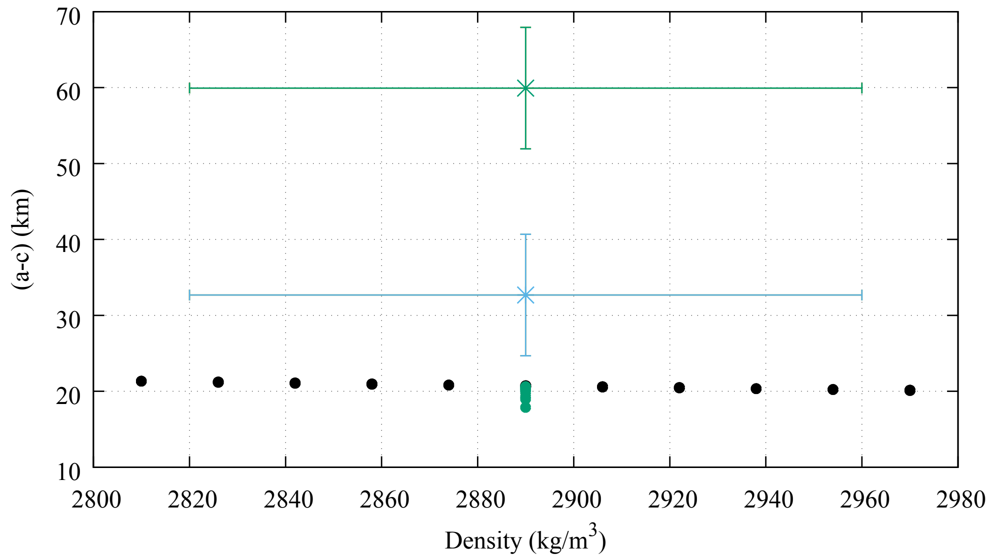

Supplementary Figure 2: **The 3D-shape of Pallas significantly deviates from hydrostatic equilibrium.** Here, the (a-c) dimensions of Pallas are shown as a function of density (green cross) compared to expected values for a similar-size body at hydrostatic equilibrium (black circles). Error bars are 3-σ uncertainties. Pallas' shape significantly deviates from equilibrium considering its current rotation period of ~7.8 h. The fitted ellipsoid in Supplementary Fig. 3 (blue cross), on the other hand, is consistent with being at equilibrium, assuming a change of rotation period of 1.6 h. This can be accounted for by the South-pole basin forming impact, or a similar-scale event. Such ellipsoid could therefore represent the original, pre-impact shape of Pallas. The model assumes a homogeneous interior for Pallas, which is supported by thermophysical modelling. The bottom green circles represent solutions for an assumed heterogeneous Pallas. In this case, (a-c) is shifted towards smaller values.

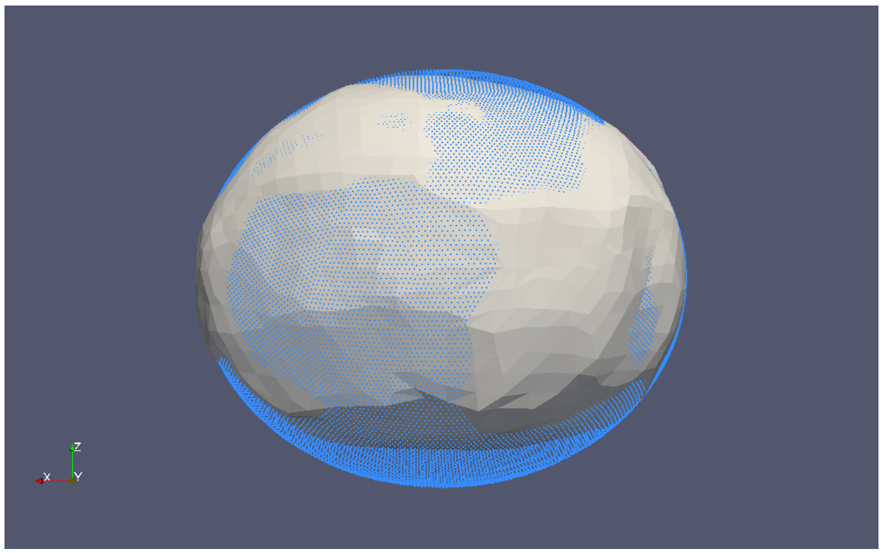

Supplementary Figure 3: **Evidence for an large impact basin on Pallas.** This equator-on view of the `ADAM` shape model highlights the flattening of the South Pole of Pallas, possibly due to the presence of a large basin alike Rheasilvia on Vesta. An ellipsoid fit rejecting southern latitudes below -31 deg. (blue) could represent the original, pre-impact shape of Pallas. Such shape would imply that the basin represents a volume of 6±1% the current volume of Pallas.

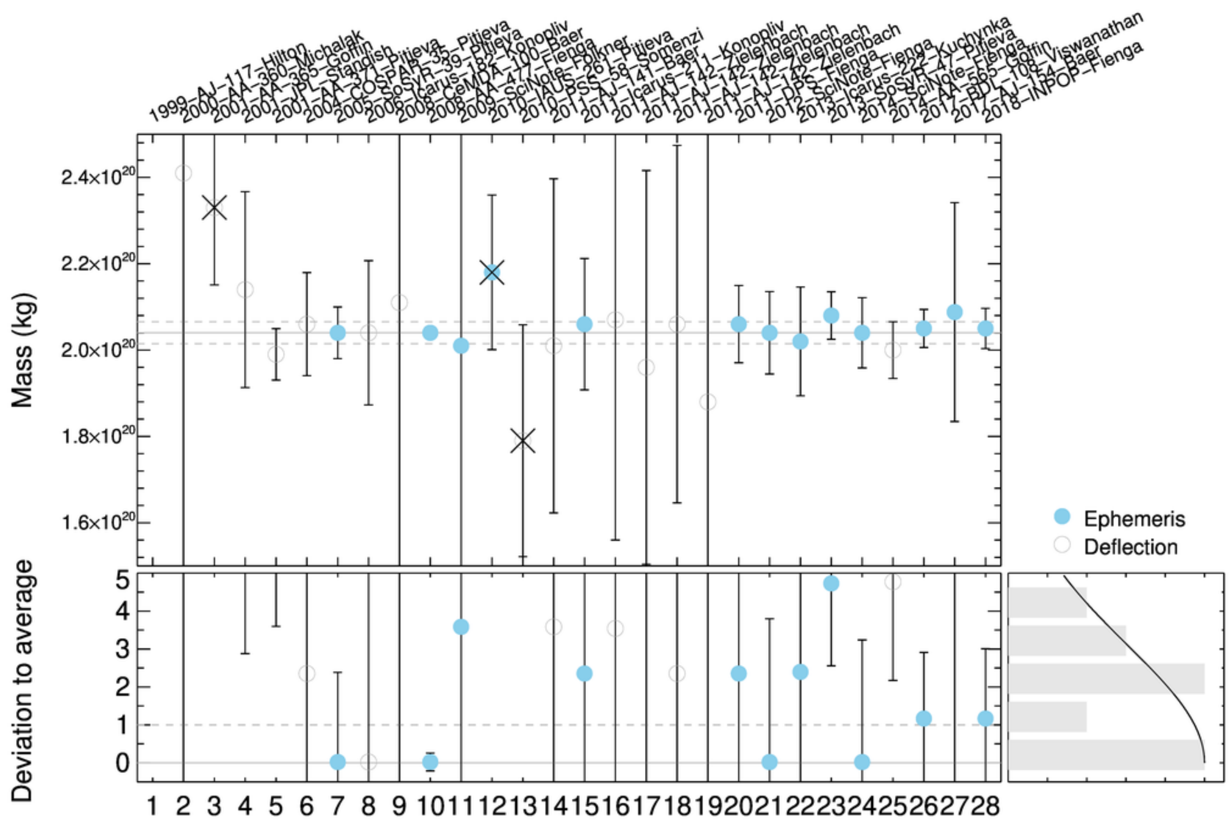

Supplementary Figure 4: **Available mass estimates for Pallas compiled from the literature.**

References are provided in Supplementary Table 4.

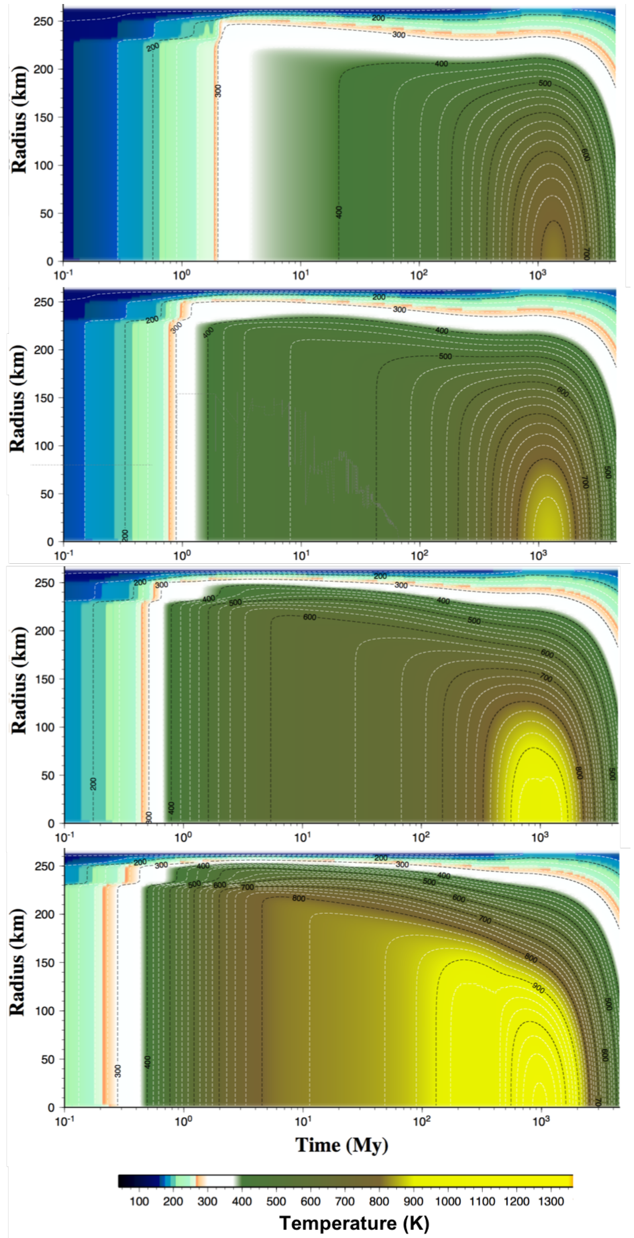

Supplementary Figure 5: **Geophysical evolution scenarios for Pallas as a function of formation time.** From top to bottom: T_0 = 3.5 Ma, T_0 = 3.0 Ma, T_0 = 2.5 Ma and T_0 = 2.0 Ma, where T_0 is the formation time in Ma after the formation of CAIs. Pallas was assumed to form as a mixture of ice and rock with a mean density of 2.9 g/cm^3. Black and white labels display isotherm values in Kelvins. Partial dehydration of Pallas' interior happens for $T_0 < 3.0$ Ma. Considering the isotopic ages of CM chondrites ($T_0 > 3.0$ Ma), Pallas' closest spectral analogues at 3 μm wavelength, this model predicts an homogeneous interior for Pallas.

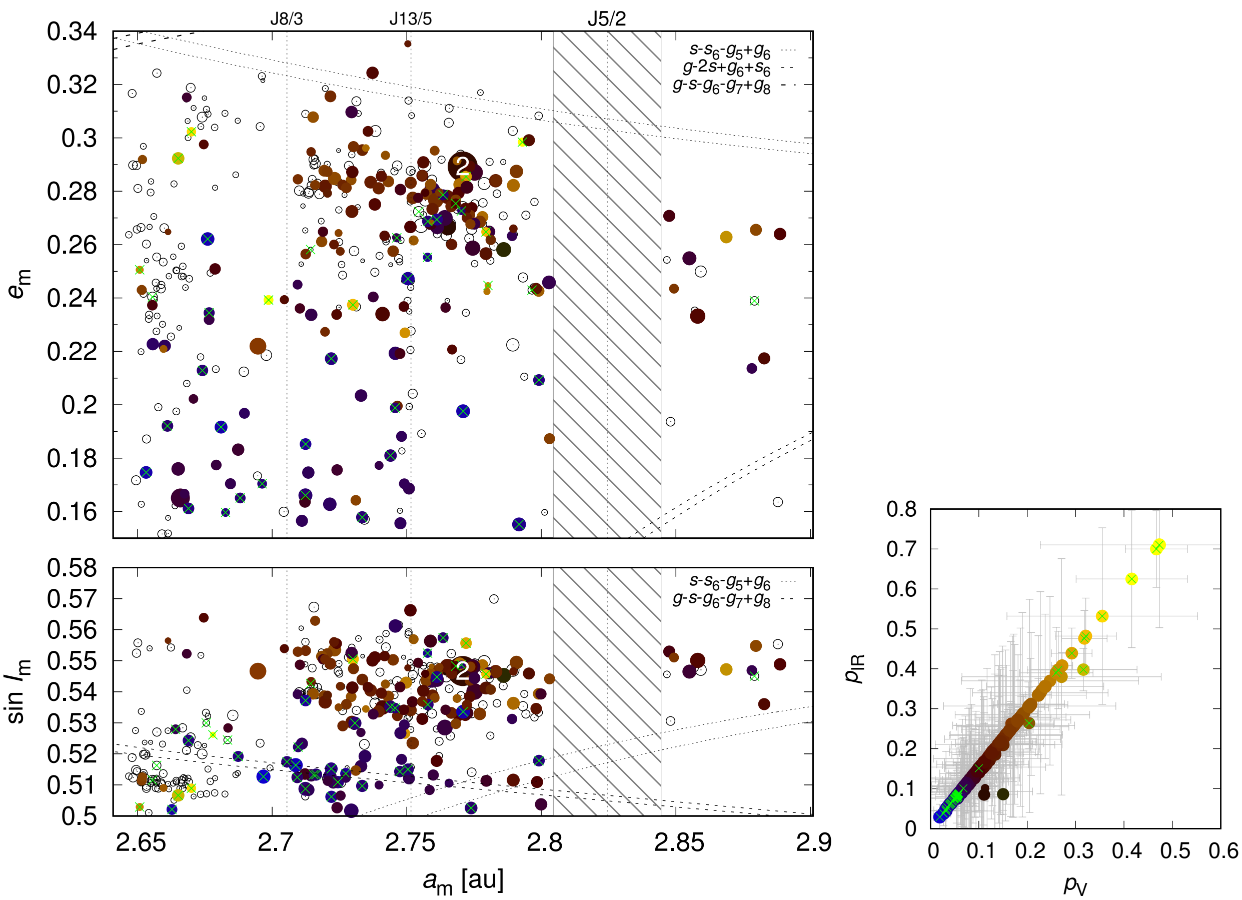

Supplementary Figure 6: **Surrounding of the Pallas family in the space of mean orbital elements.** All asteroids within the range of osculating $a \in (2.649; 2.95)$ au, $e \in (0.05; 0.4)$, and $I \in (29°; 38°)$ are shown. Colours indicate the geometric albedo p_V, when known, following the right panel showing p_V *vs.* p_{IR} (blue corresponds to the lowest albedo values and yellow to highest ones). Symbol sizes are proportional to diameters. Plausible interlopers are also indicated (green crosses). Several mean-motion resonances J8/3, J13/5 and J5/2 (dotted or hatched) and secular resonances $s - s_6 - g_5 + g_6$, $g - s - g_6 - g_7 + g_8$, $g - 2s + g_6 + s_6$ (dashed) can affect the orbits of the family members.

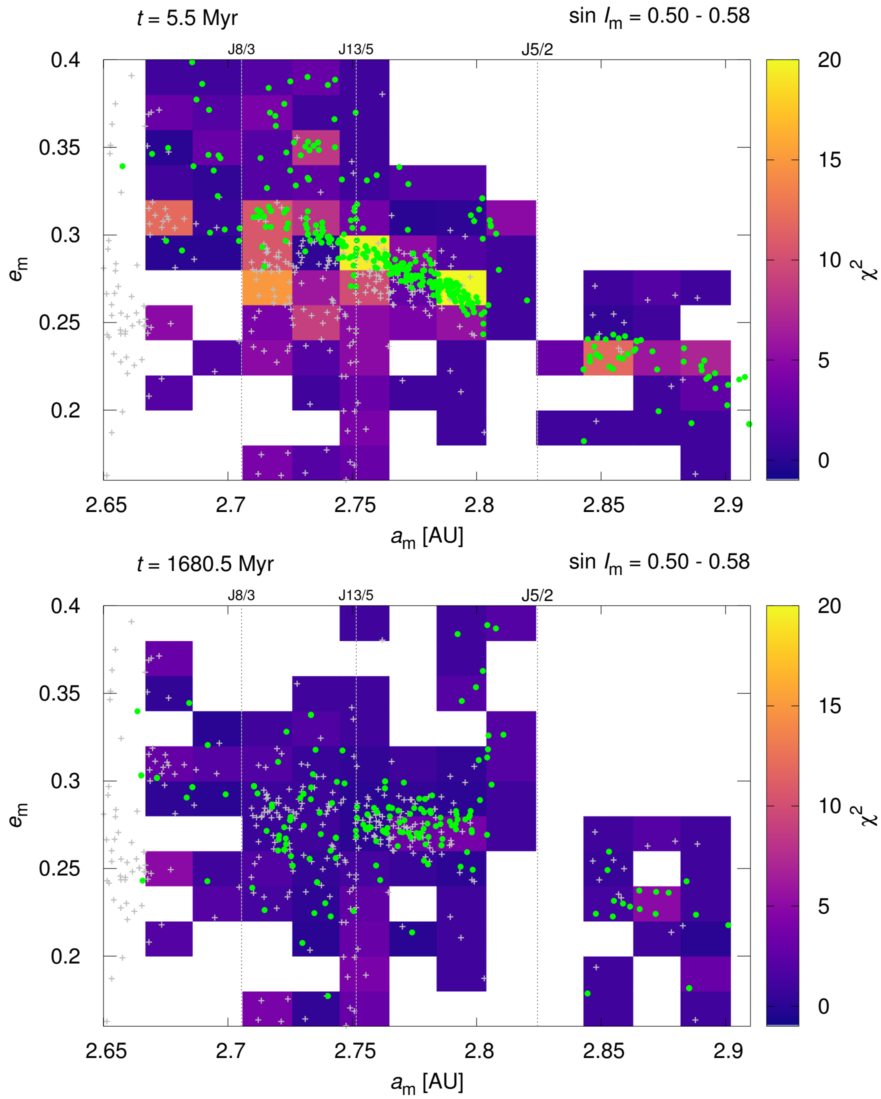

Supplementary Figure 7: **Orbital distributions of the synthetic Pallas family (green dots), compared to the observed family (gray crosses).** The families are shown in mean semimajor axis a_m *vs.* mean eccentricity e_m. The underlying boxes are used to count bodies and compute the χ^2 used to evaluate the goodness of fit between simulations and observations. The colour scale indicates individual contributions to the χ^2 sum. The situation at the beginning of the simulation (top) and the best fit at $t = 1.68\,\mathrm{Ga}$ (bottom) are shown. The discrepancy below the J8/3 resonance is due to contamination from the Barcelona family, and at low eccentricity $e_\mathrm{m} < 0.2$ due to the Brucato one[1].

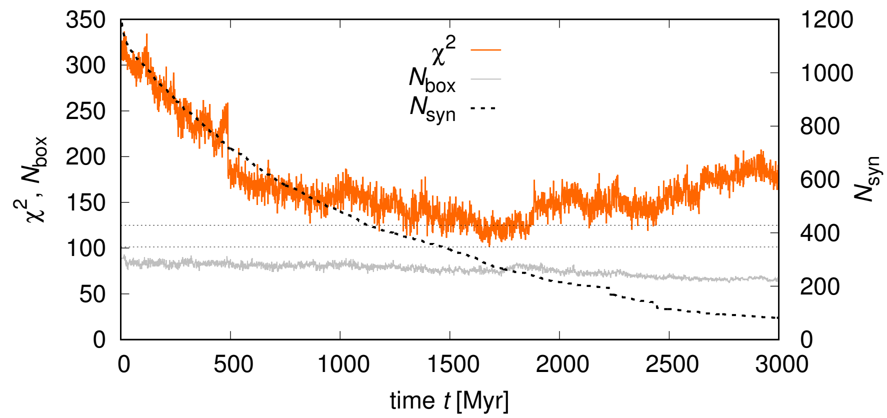

Supplementary Figure 8: **Goodness of fit of the synthetic family in our N-body simulations to the observed Pallas family.** The value of χ^2 *vs.* time t is shown together with the number of boxes $N_{\rm box}$ in which synthetic and observed bodies were counted. For a perfect fit, $\chi^2 \simeq N_{\rm box}$. In our case, the ratio reaches $\chi^2/N_{\rm box} \simeq 1.35$. The horizontal dotted lines correspond to the best-fit $\chi^2 = 101$ and to a typical scatter of $\chi^2(t)$. The number of synthetic bodies $N_{\rm syn}(t)$ is also plotted (using the other ordinate).

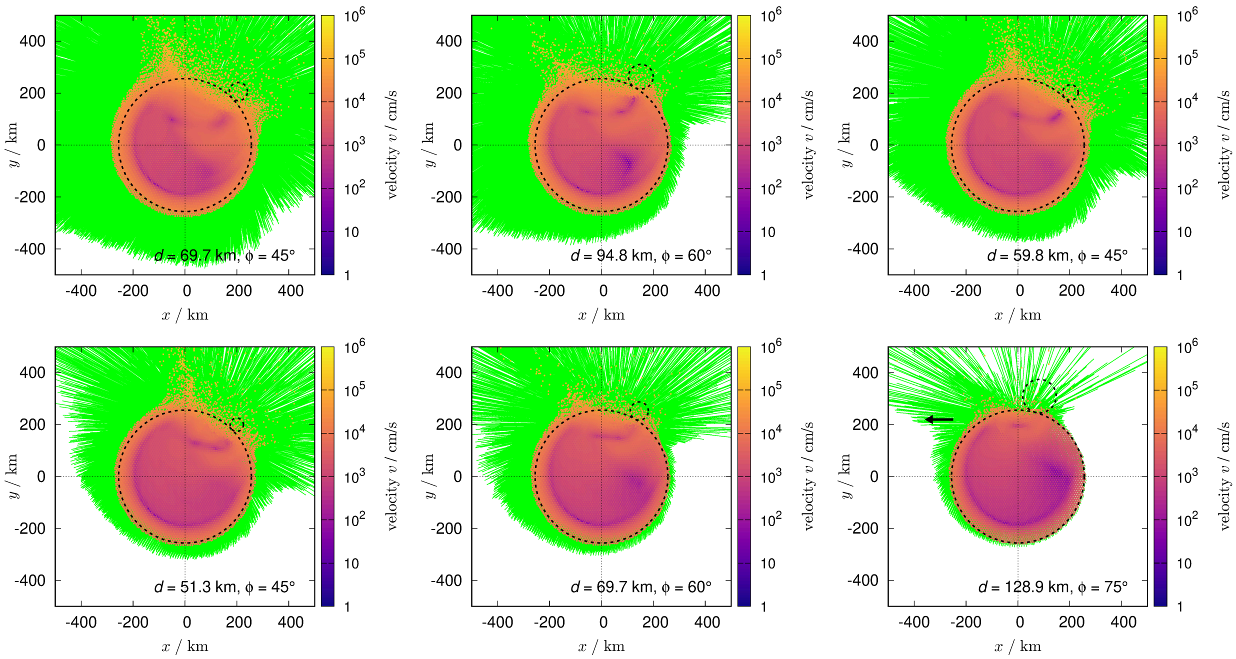

Supplementary Figure 9: **Intermediate results of the SPH simulations of the impact at the origin of the Pallas family.** The situation is shown as a cut-away in the (x, y) plane, with a projectile flying in $-\hat{x}$ direction. At the time $t = 200\,\mathrm{s}$, the fragmentation phase has ended and the projectile is already gone. The impact velocity was $v_{\mathrm{imp}} = 12\,\mathrm{km\,s^{-1}}$, target size $D = 513\,\mathrm{km}$; several combinations of the projectile sizes $d = 51.3$, 69.7, $94.8\,\mathrm{km}$, and the impact angles $\phi = 45°$, $60°$, $75°$ were tested. The colour scale corresponds to the (logarithm of) fragment velocity. Black dotted circles indicate the target and projectile at the point of first contact. Green lines show typical distances fragments would fly on the time scale of their free fall in the given gravity field, $g \doteq 0{,}21\,\mathrm{m\,s^{-2}}$. The simulations are ordered according to their specific energy $Q/Q^{\star}_{D}$.

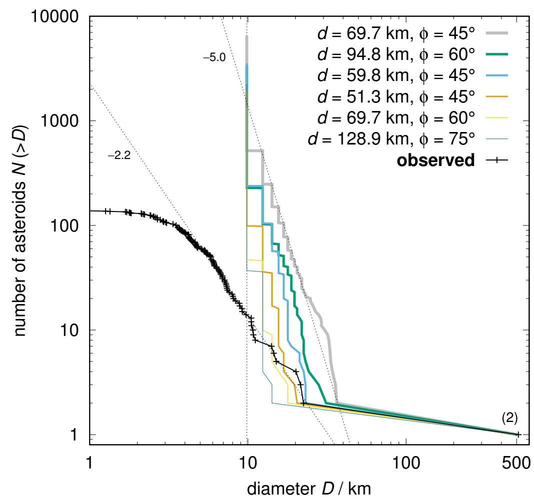

Supplementary Figure 10: **Cumulative size-frequency distribution (SFD) of synthetic families (colours), compared to the observed Pallas family (black).** The SFDs were computed after the gravitational reaccumulation ended. The observed slope is shallow (-2.2) while the synthetic ones are steep (about -5.0), implying significant subsequent collisional and orbital evolution of the fragment population. The order of the simulations is the same as in Supplementary Fig. 9.

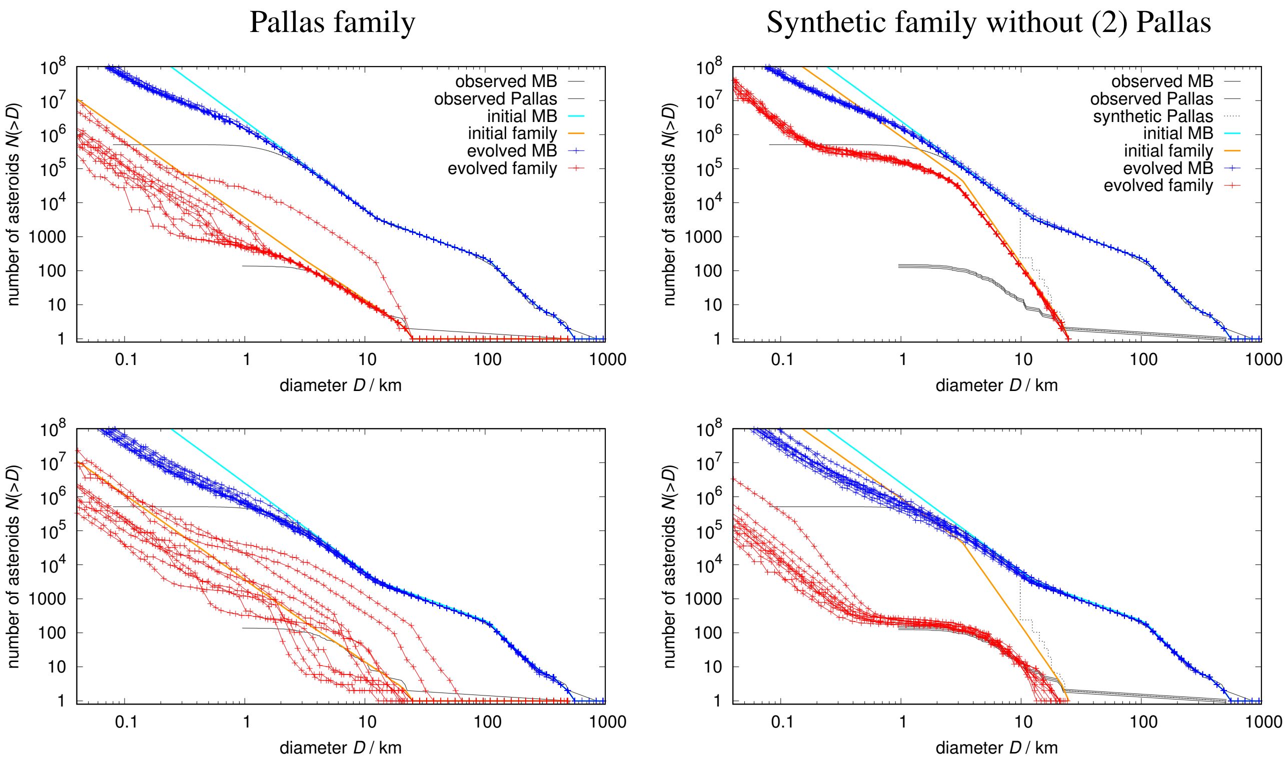

Supplementary Figure 11: **Cumulative size-frequency distributions** $N(>D)$ **resulting from two Monte-Carlo collisional models:** the main belt and the Pallas family (left column); the main belt and a synthetic family without the largest remnant (2) Pallas (right column). The main belt SFD is plotted in blue and the family SFD in red; the respective initial conditions in cyan and orange, and the observations are in gray; the bend at around $D \simeq 1\,\mathrm{km}$ is mostly due to the observational incompleteness. The situation at time $t = 100\,\mathrm{Ma}$ (top row), and $t = 2000\,\mathrm{Ma}$ (bottom row) is shown. There are always 10 runs with a different random seed in order to see lower-probability events.

Supplementary Table 1: **Identified craters on Pallas.** D_c is the diameter and (λ, β) the planetocentric coordinates. Craters detected at multiple rotation phase angles were attributed names, whereas those detected at a single epoch are designated by letters. Because (2) Pallas was named after Pallas Athena, the greek goddess of war, we decided to name its main craters after ancient greek names of weapons.

#	**Name**	D_c **(km)**	(λ, β) (°)
1	Hoplon	115	(230, -58)
2	Doru	110	(76, -40)
3	Sfendnai	110	(34, -35)
4	Akontia	100	(130, -68)
5	Xyston	95	(148, -43)
6	Toxa	78	(119, -48)
7	Xiphos	60	(247, -42)
8	Sarissa	54	(222, -44)
9	Kopis	53	(297, -76)
10	Aklys	92	(298, 38)
11	Spatha	68	(274, 50)
12	Sica	73	(246, 54)
13	Pilum	82	(185, 45)
14	Scutum	68	(350, 63)

Continued on next page

Supplementary Table 1 – *Continued from previous page*

#	**Name**	D **(km)**	(λ, β) (°)
15	Falcata	46	(224, 47)
16	Makhaira	49	(184, 60)
17	A	78	(184, -14)
18	B	67	(194, -42)
19	C	77	(7, 2)
20	D	61	(17, -12)
21	E	92	(4, -38)
22	F	46	(299, -25)
23	G	27	(322, -52)
24	H	57	(15, -45)
25	J	49	(153, 26)
26	K	56	(121, -2)
27	L	48	(23, 43)
28	M	50	(325, 50)
29	N	37	(355, 70)
30	O	45	(199, 54)
31	P	54	(214, 64)
32	Q	58	(321, 27)

Continued on next page

Supplementary Table 1 – *Continued from previous page*

#	**Name**	D **(km)**	(λ, β) (°)
33	R	64	(80, 33)
34	S	52	(86, 50)
35	U	42	(262, 70)
36	V	72	(277, 36)

Supplementary Table 2: **List of disk-resolved images used for `ADAM` shape modelling.** For each observation, the table provides the epoch, the instrument, the filter, the exposure time, the airmass, the distance to the Earth Δ and the Sun r, the phase angle α, the angular diameter D_a, the survey ID, and the name of the PI of the data.

Date	**UT**	**Instrument**	**Filter**	**Exp (s)**	**Airmass**	Δ **(AU)**	r **(AU)**	α (°)	D_a (")	**Survey ID**	**PI**
2002-05-08	14:58:36	Keck/NIRC2	H	1	1.09	3.38	3.41	17.1	0.213	C74N2	Margot
2003-10-10	11:58:46	Keck/NIRC2	Kp	20	1.28	1.80	2.73	9.4	0.400	Engineering	–
2003-10-12	09:12:42	Keck/NIRC2	Kp	2	1.40	1.80	2.73	9.5	0.400	Engineering	–
2003-10-12	11:11:03	Keck/NIRC2	Kp	2	1.25	1.80	2.73	9.5	0.400	Engineering	–
2003-10-12	11:27:02	Keck/NIRC2	Kp	2	1.26	1.80	2.73	9.5	0.400	Engineering	–
2006-08-16	06:48:36	Keck/NIRC2	Ks	1	1.00	2.76	3.35	15.5	0.261	U145N2	Nelson
2006-08-16	07:29:28	Keck/NIRC2	Ks	1	1.42	2.76	3.35	15.5	0.261	U145N2	Nelson
2006-08-16	07:44:38	Keck/NIRC2	Ks	1	1.03	2.76	3.35	15.5	0.261	U145N2	Nelson
2006-08-16	08:11:04	Keck/NIRC2	Ks	1	1.06	2.76	3.35	15.5	0.261	U145N2	Nelson
2006-08-16	08:41:54	Keck/NIRC2	Ks	0	1.13	2.76	3.35	15.5	0.261	U145N2	Nelson
2006-08-16	08:45:03	Keck/NIRC2	Ks	1	1.13	2.76	3.35	15.5	0.261	U145N2	Nelson

Continued on next page

Supplementary Table 2 – *Continued from previous page*

Date	**UT**	**Instrument**	**Filter**	**Exp (s)**	**Airmass**	Δ **(AU)**	r **(AU)**	α (°)	D_{a} (")	**Survey ID**	**PI**
2006-08-16	09:17:31	Keck/NIRC2	Ks	1	1.23	2.76	3.35	15.5	0.261	U145N2	Nelson
2006-08-16	10:05:32	Keck/NIRC2	Ks	1	1.47	2.76	3.35	15.5	0.261	U145N2	Nelson
2006-08-16	10:21:42	Keck/NIRC2	Ks	1	1.58	2.76	3.35	15.5	0.261	U145N2	Nelson
2007-07-12	12:56:58	Keck/NIRC2	Kp	2	1.04	2.69	3.31	15.5	0.268	Engineering	–
2007-07-12	13:01:32	Keck/NIRC2	Kp	2	1.04	2.69	3.31	15.5	0.268	Engineering	–
2007-07-12	13:15:54	Keck/NIRC2	Kp	2	1.03	2.69	3.31	15.5	0.268	Engineering	–
2007-11-01	06:04:39	Keck/NIRC2	Kp	2	1.12	2.64	3.16	16.9	0.273	Engineering	–
2017-10-08	4:56:05	VLT/SPHERE	N_R	121	1.13	1.77	2.59	15.1	0.407	199.C-0074	Vernazza
2017-10-08	4:58:16	VLT/SPHERE	N_R	121	1.12	1.77	2.59	15.1	0.407	199.C-0074	Vernazza
2017-10-08	5:00:27	VLT/SPHERE	N_R	121	1.12	1.77	2.59	15.1	0.407	199.C-0074	Vernazza
2017-10-08	5:02:36	VLT/SPHERE	N_R	121	1.11	1.77	2.59	15.1	0.407	199.C-0074	Vernazza
2017-10-08	5:04:46	VLT/SPHERE	N_R	121	1.11	1.77	2.59	15.1	0.407	199.C-0074	Vernazza
2017-10-11	5:04:27	VLT/SPHERE	N_R	121	1.08	1.75	2.59	14.8	0.411	199.C-0074	Vernazza

Continued on next page

Supplementary Table 2 – *Continued from previous page*

Date	UT	Instrument	Filter	Exp (s)	Airmass	Δ (AU)	r (AU)	α (°)	D_a (")	Survey ID	PI
2017-10-11	5:06:39	VLT/SPHERE	N_R	121	1.08	1.75	2.59	14.8	0.411	199.C-0074	Vernazza
2017-10-11	5:08:49	VLT/SPHERE	N_R	121	1.08	1.75	2.59	14.8	0.411	199.C-0074	Vernazza
2017-10-11	5:11:00	VLT/SPHERE	N_R	121	1.07	1.75	2.59	14.8	0.411	199.C-0074	Vernazza
2017-10-11	5:13:10	VLT/SPHERE	N_R	121	1.07	1.75	2.59	14.8	0.411	199.C-0074	Vernazza
2017-10-11	6:00:47	VLT/SPHERE	N_R	121	1.02	1.75	2.59	14.8	0.411	199.C-0074	Vernazza
2017-10-11	6:02:58	VLT/SPHERE	N_R	121	1.02	1.75	2.59	14.8	0.411	199.C-0074	Vernazza
2017-10-11	6:05:07	VLT/SPHERE	N_R	121	1.01	1.75	2.59	14.8	0.411	199.C-0074	Vernazza
2017-10-11	6:07:17	VLT/SPHERE	N_R	121	1.01	1.75	2.59	14.8	0.411	199.C-0074	Vernazza
2017-10-11	6:09:28	VLT/SPHERE	N_R	121	1.01	1.75	2.59	14.8	0.411	199.C-0074	Vernazza
2017-10-11	6:51:15	VLT/SPHERE	N_R	121	1.01	1.75	2.59	14.8	0.411	199.C-0074	Vernazza
2017-10-11	6:53:27	VLT/SPHERE	N_R	121	1.01	1.75	2.59	14.8	0.411	199.C-0074	Vernazza
2017-10-11	6:55:36	VLT/SPHERE	N_R	121	1.01	1.75	2.59	14.8	0.411	199.C-0074	Vernazza
2017-10-11	6:57:47	VLT/SPHERE	N_R	121	1.01	1.75	2.59	14.8	0.411	199.C-0074	Vernazza

Continued on next page

Supplementary Table 2 – *Continued from previous page*

Date	**UT**	**Instrument**	**Filter**	**Exp (s)**	**Airmass**	Δ **(AU)**	r **(AU)**	α (°)	D_a (")	**Survey ID**	**PI**
2017-10-11	6:59:57	VLT/SPHERE	N_R	121	1.01	1.75	2.59	14.8	0.411	199.C-0074	Vernazza
2017-10-28	8:28:03	VLT/SPHERE	N_R	121	1.35	1.70	2.54	14.4	0.423	199.C-0074	Vernazza
2017-10-28	8:30:14	VLT/SPHERE	N_R	121	1.37	1.70	2.54	14.4	0.423	199.C-0074	Vernazza
2017-10-28	8:32:24	VLT/SPHERE	N_R	121	1.38	1.70	2.54	14.4	0.423	199.C-0074	Vernazza
2017-10-28	8:34:34	VLT/SPHERE	N_R	121	1.39	1.70	2.54	14.4	0.423	199.C-0074	Vernazza
2017-10-28	8:36:43	VLT/SPHERE	N_R	121	1.40	1.70	2.54	14.4	0.423	199.C-0074	Vernazza
2017-11-03	3:17:46	VLT/SPHERE	N_R	121	1.08	1.70	2.53	14.8	0.423	199.C-0074	Vernazza
2017-11-03	3:19:57	VLT/SPHERE	N_R	121	1.07	1.70	2.53	14.8	0.423	199.C-0074	Vernazza
2017-11-03	3:22:08	VLT/SPHERE	N_R	121	1.07	1.70	2.53	14.8	0.423	199.C-0074	Vernazza
2017-11-03	3:24:17	VLT/SPHERE	N_R	121	1.07	1.70	2.53	14.8	0.423	199.C-0074	Vernazza
2017-11-03	3:26:27	VLT/SPHERE	N_R	121	1.06	1.70	2.53	14.8	0.423	199.C-0074	Vernazza
2019-03-14	5:36:08	VLT/SPHERE	N_R	45	1.37	1.62	2.47	14.7	0.444	199.C-0074	Vernazza
2019-03-14	5:37:02	VLT/SPHERE	N_R	45	1.37	1.62	2.47	14.7	0.444	199.C-0074	Vernazza

Continued on next page

Supplementary Table 2 – *Continued from previous page*

Date	**UT**	**Instrument**	**Filter**	**Exp (s)**	**Airmass**	Δ **(AU)**	r **(AU)**	α (°)	D_a (”)	**Survey ID**	**PI**
2019-03-14	5:37:56	VLT/SPHERE	N_R	45	1.37	1.62	2.47	14.7	0.444	199.C-0074	Vernazza
2019-03-14	5:38:48	VLT/SPHERE	N_R	45	1.36	1.62	2.47	14.7	0.444	199.C-0074	Vernazza
2019-03-14	5:39:41	VLT/SPHERE	N_R	45	1.36	1.62	2.47	14.7	0.444	199.C-0074	Vernazza
2019-03-15	6:55:56	VLT/SPHERE	N_R	45	1.22	1.62	2.48	14.4	0.444	199.C-0074	Vernazza
2019-03-15	6:56:49	VLT/SPHERE	N_R	45	1.22	1.62	2.48	14.4	0.444	199.C-0074	Vernazza
2019-03-15	6:57:42	VLT/SPHERE	N_R	45	1.22	1.62	2.48	14.4	0.444	199.C-0074	Vernazza
2019-03-15	6:58:36	VLT/SPHERE	N_R	45	1.22	1.62	2.48	14.4	0.444	199.C-0074	Vernazza
2019-03-15	6:59:27	VLT/SPHERE	N_R	45	1.22	1.62	2.48	14.4	0.444	199.C-0074	Vernazza
2019-03-24	9:24:22	VLT/SPHERE	N_R	45	1.72	1.59	2.50	12.1	0.453	199.C-0074	Vernazza
2019-03-24	9:25:17	VLT/SPHERE	N_R	45	1.72	1.59	2.50	12.1	0.453	199.C-0074	Vernazza
2019-03-24	9:26:10	VLT/SPHERE	N_R	45	1.73	1.59	2.50	12.1	0.453	199.C-0074	Vernazza
2019-03-24	9:27:02	VLT/SPHERE	N_R	45	1.74	1.59	2.50	12.1	0.453	199.C-0074	Vernazza
2019-03-24	9:27:56	VLT/SPHERE	N_R	45	1.74	1.59	2.50	12.1	0.453	199.C-0074	Vernazza

Continued on next page

Supplementary Table 2 – *Continued from previous page*

Date	**UT**	**Instrument**	**Filter**	**Exp (s)**	**Airmass**	**Δ (AU)**	**r (AU)**	**α (°)**	**D_a (”)**	**Survey ID**	**PI**
2019-03-25	3:58:30	VLT/SPHERE	N_R	45	1.71	1.59	2.50	12.0	0.453	199.C-0074	Vernazza
2019-03-25	3:59:24	VLT/SPHERE	N_R	45	1.70	1.59	2.50	12.0	0.453	199.C-0074	Vernazza
2019-03-25	4:00:18	VLT/SPHERE	N_R	45	1.70	1.59	2.50	12.0	0.453	199.C-0074	Vernazza
2019-03-25	4:01:11	VLT/SPHERE	N_R	45	1.69	1.59	2.50	12.0	0.453	199.C-0074	Vernazza
2019-03-25	4:02:04	VLT/SPHERE	N_R	45	1.69	1.59	2.50	12.0	0.453	199.C-0074	Vernazza
2019-03-28	3:35:44	VLT/SPHERE	N_R	45	1.81	1.59	2.51	11.4	0.453	199.C-0074	Vernazza
2019-03-28	3:36:41	VLT/SPHERE	N_R	45	1.81	1.59	2.51	11.4	0.453	199.C-0074	Vernazza
2019-03-28	3:37:34	VLT/SPHERE	N_R	45	1.80	1.59	2.51	11.4	0.453	199.C-0074	Vernazza
2019-03-28	3:38:26	VLT/SPHERE	N_R	45	1.79	1.59	2.51	11.4	0.453	199.C-0074	Vernazza
2019-03-28	3:39:19	VLT/SPHERE	N_R	45	1.79	1.59	2.51	11.4	0.453	199.C-0074	Vernazza

Supplementary Table 3: **List of optical disk-integrated lightcurves used for `ADAM` shape modelling.** For each lightcurve, the table provides the epoch, the number of individual measurements N_p, the distance to the Earth Δ and the Sun r, the phase angle α, the photometric filter and the bibliographic reference.

N	Epoch	N_p	Δ (AU)	r (AU)	α (°)	Filter	Reference
1	1951-06-30.4	31	2.66	3.41	13.0	V	[3]
2	1956-08-26.3	63	2.42	3.36	7.4	V	[4]
3	1956-08-29.2	42	2.42	3.36	7.7	V	[4]
4	1956-08-31.2	32	2.43	3.36	7.9	V	[4]
5	1963-02-04.6	60	1.44	2.13	23.3	V	[5]
6	1963-02-12.6	49	1.46	2.12	24.1	V	[5]
7	1963-02-27.6	53	1.54	2.12	25.7	V	[5]
8	1963-02-28.5	31	1.54	2.12	25.8	V	[5]
9	1965-07-28.7	52	2.54	3.42	9.8	V	[6]
10	1965-08-06.9	64	2.52	3.42	9.3	V	[7]
11	1965-08-23.7	63	2.55	3.41	10.2	V	[6]
12	1965-08-24.6	51	2.55	3.41	10.3	V	[6]
13	1968-02-11.1	20	1.37	2.21	17.1	V	[8]
14	1968-02-17.1	11	1.33	2.22	14.3	V	[8]

Supplementary Table 3: continued.

N	Epoch	N_p	Δ (AU)	r (AU)	α (°)	Filter	Reference
15	1968-03-13.9	21	1.27	2.27	0.2	V	[8]
16	1968-03-30.0	57	1.34	2.30	9.1	V	[8]
17	1968-03-30.9	67	1.35	2.30	9.6	V	[8]
18	1968-04-21.9	41	1.56	2.35	18.6	V	[8]
19	1968-04-22.9	52	1.57	2.35	18.9	V	[8]
20	1969-08-26.9	50	2.91	3.34	16.9	V	[8]
21	1970-07-12.0	33	2.69	3.35	14.8	V	[9]
22	1970-07-29.0	53	2.50	3.33	11.5	V	[9]
23	1970-08-06.0	59	2.43	3.32	9.6	V	[9]
24	1970-08-27.0	77	2.32	3.30	5.3	V	[9]
25	1970-10-04.9	82	2.46	3.25	12.6	V	[9]
26	1971-11-28.2	41	1.60	2.34	19.6	V	[8]
27	1971-11-29.2	91	1.60	2.33	19.7	V	[8]
28	1971-11-30.2	23	1.60	2.33	19.7	V	[8]
29	1973-04-04.1	45	1.85	2.66	15.1	C	[10]
30	1973-04-05.0	100	1.84	2.66	15.0	C	[10]
31	1973-04-07.1	60	1.84	2.67	14.7	C	[10]
32	1973-04-08.1	29	1.84	2.67	14.6	V	[10]

Supplementary Table 3: continued.

N	Epoch	N_p	Δ (AU)	r (AU)	α (°)	Filter	Reference
33	1973-04-27.0	73	1.86	2.72	13.5	V	[11]
34	1973-05-08.0	105	1.91	2.74	14.2	V	[11]
35	1973-05-13.3	56	1.94	2.76	14.8	V	[12]
36	1973-05-14.0	106	1.94	2.76	14.9	V	[11]
37	1973-06-16.3	56	2.26	2.84	19.0	V	[12]
38	1974-07-10.9	60	2.59	3.41	11.7	V	[11]
39	1974-07-13.9	73	2.58	3.41	11.5	V	[11]
40	1974-07-14.9	56	2.58	3.41	11.4	V	[11]
41	1974-07-15.9	31	2.58	3.41	11.3	V	[11]
42	1974-07-18.9	30	2.57	3.41	11.1	V	[11]
43	1974-08-20.0	49	2.64	3.42	12.4	V	[10]
44	1982-03-21.3	34	1.48	2.42	9.4	V	[13]
45	1982-03-21.4	93	1.48	2.42	9.3	V	[13]
46	1982-03-22.2	37	1.48	2.43	9.2	V	[14]
47	1983-05-12.3	5	2.82	3.29	16.9	V	[13]
48	1983-05-12.4	10	2.82	3.29	16.9	V	[13]
49	1983-05-12.5	5	2.82	3.29	16.9	V	[13]
50	1983-07-17.0	86	2.57	3.36	12.5	V	[15]

Supplementary Table 3: continued.

N	Epoch	N_p	Δ (AU)	r (AU)	α (°)	Filter	Reference
51	1983-07-19.0	52	2.57	3.36	12.6	V	[15]
52	1983-07-21.0	44	2.58	3.36	12.6	V	[15]
53	1984-07-04.4	77	2.82	3.29	17.0	V	[16]
54	1984-09-03.9	37	2.21	3.21	3.1	V	[17]
55	1985-11-29.3	8	1.56	2.23	22.5	V	[18]
56	1985-11-30.3	9	1.56	2.23	22.4	V	[18]
57	1985-12-01.2	8	1.56	2.23	22.4	V	[18]
58	1986-01-01.2	27	1.48	2.18	22.2	V	[19]
59	1986-01-11.2	27	1.49	2.17	22.7	V	[18]
60	1986-01-12.2	38	1.49	2.17	22.8	V	[18]
61	1986-01-17.2	31	1.49	2.16	23.1	V	[18]

Supplementary Table 4: **Mass estimates ($\mathcal{M}$) of (2) Pallas collected in the literature.** The $3\,\sigma$ uncertainty, method, selection flag (accepted ✓ or rejected ✗), and bibliographic reference are reported for each estimate. The methods are *defl*: Deflection, *ephem*: Ephemeris.

#	$\mathcal{M}$ ($\times 10^{20}$ kg)	Method	Sel.	Reference
1	3.16 ± 0.30	*defl*	✗	[21]
2	2.41 ± 1.55	*defl*	✓	[22]
3	2.33 ± 0.18	*defl*	✗	[23]
4	2.14 ± 0.23	*defl*	✓	[24]
5	1.99 ± 0.06	*defl*	✓	[25]
6	2.06 ± 0.12	*defl*	✓	[26]
7	2.04 ± 0.06	*ephem*	✓	[27]
8	2.04 ± 0.17	*defl*	✓	[28]
9	2.11 ± 0.78	*defl*	✓	[29]
10	2.04 ± 0.01	*ephem*	✓	[30]
11	2.01 ± 0.60	*ephem*	✓	[31]
12	2.18 ± 0.18	*ephem*	✗	[32]
13	1.79 ± 0.27	*defl*	✗	[33]
14	2.01 ± 0.39	*defl*	✓	[34]
15	2.06 ± 0.15	*ephem*	✓	[35]
16	2.07 ± 0.51	*defl*	✓	[36]

Continued on next page

Supplementary Table 4 – *Continued from previous page*

#	$\mathcal{M}$ ($\times 10^{20}$ kg)	Method	Sel.	Reference
17	1.96 ± 0.46	*defl*	✓	[36]
18	2.06 ± 0.41	*defl*	✓	[36]
19	1.88 ± 0.71	*defl*	✓	[36]
20	2.06 ± 0.09	*ephem*	✓	[37]
21	2.04 ± 0.10	*ephem*	✓	[38]
22	2.02 ± 0.13	*ephem*	✓	[39]
23	2.08 ± 0.05	*ephem*	✓	[40]
24	2.04 ± 0.08	*ephem*	✓	[41]
25	2.00 ± 0.07	*defl*	✓	[42]
26	2.05 ± 0.04	*ephem*	✓	[43]
27	2.09 ± 0.25	*ephem*	✓	[44]
28	2.05 ± 0.05	*ephem*	✓	[45]
	2.04 ± 0.03	Average		

Supplementary Table 5: **Input parameters for the Monte-Carlo collisional models of Ceres, Vesta and Pallas.** P_i denotes the intrinsic collisional probability, v_imp the median velocity of collisions with the main belt population, D_t the target diameter, ρ the bulk density, and d_p the projectile diameter needed to create a crater with diameter $D_\mathrm{c} \geq 40\,\mathrm{km}$ (inferred from the π-scaling[2]).

	P_i	v_imp	D_t	ρ	d_p
	$10^{-18}\,\mathrm{km^{-2}\,a^{-1}}$	$\mathrm{km\,s^{-1}}$	km	$\mathrm{g\,cm^{-3}}$	km
(1) Ceres	3.58	5.07	946	2.16	3.78
(2) Pallas	2.17	11.49	513	2.89	2.42
(4) Vesta	2.92	5.29	525	3.46	4.27

Supplementary Table 6: **Initial conditions and selected results of the SPH simulations.** d_p denotes the projectile diameter, ϕ_{imp} the impact angle, D_{pb} the parent body diameter, Q_{eff} the effective strength[20], $Q^\star_D$ the scaling law, M_{ex} the excavated mass, M_{ej} the ejected mass. The impact velocity was $v_{imp} = 12\,\mathrm{km\,s^{-1}}$ in all cases.

d_p km	ϕ_{imp} deg	$\log(d_p/D_{pb})$	$Q_{eff}/Q^\star_D$	$\frac{M_{ex}}{M_{pb}}$	$\frac{M_{ej}}{M_{pb}}$
69.7	45	2.6	0.106	0.0467	0.0581
94.8	60	2.2	0.103⋆	0.0241	0.0280
59.8	45	2.8	0.067	0.0270	0.0284
51.3	45	3.0	0.042	0.0156	0.0148
69.7	60	2.6	0.059⋆	0.0104	0.0100
128.9	75	1.8	0.024⋆	0.0022	0.0013

Supplementary Table 7: **Input parameters for radioisotope decay heat calculation.** See Castillo-Rogez et al. (2007)[46] for references.

Parent Nuclide	^{26}Al	^{60}Fe	^{40}K	^{232}Al	^{235}U	^{238}U
Initial Isotopic Abundance (wt.%)	$5\text{x}10^{-5}$	10^{-7}	0.01176	100	0.71	99.28
Half Life (Ma)	0.72	1.5	1277	14020	703.71	4468
Specific Heat Production (W/kg)	0.146	0.070	$29.17\text{x}10^{-6}$	$26.38\text{x}10^{-6}$	$568.7\text{x}10^{-6}$	$94.65\text{x}10^{-6}$

1. Nesvorný, D., Brož, M. & Carruba, V. Identification and Dynamical Properties of Asteroid Families. In *Asteroids IV*, 297–321 (University of Arizona Press, Tucson, 2015).

2. Melosh, H. J. *Impact cratering: A geologic process* (New York, Oxford University Press, 1989).

3. Groeneveld, I. & Kuiper, G. P. Photometric Studies of Asteroids. II. *Astrophys. J.* **120**, 529 (1954).

4. Wood, X. H. J. & Kuiper, G. P. Photometric Studies of Asteroids. *Astrophys. J.* **137**, 1279 (1963).

5. Chang, Y. C. & S., C. C. Unknown. *Acta Astron. Sinica* **11**, 139 (1963).

6. Chang, Y. C. *et al.* Light curves of Asteroids (IV). *Chinese Astron. Astrophys.* **5**, 434–437 (1981).

Supplementary Table 8: **Thermophysical material properties assumed in this study.** Hydrohalite is taken as a reference for the salts since it is the dominant species. Ice thermal conductivity has a high dependence on temperature. On the other hand, the thermal conductivities of clathrates show a weak dependence on temperature (see Durham et al. 2010[47] for a review). Both species have high specific heat capacities.

Phase	ρ kg m^{-3}	κ W m^{-1} K^{-1}	c_p J kg^{-1} K^{-1}	Reference
Ice	917	$0.4685 + 488.12/T$	$185 + 7.037 \cdot T$	[48]
Clathrate hydrate	1000	0.64	$494 + 6.1 \cdot T$	[49]
Salt (hydrohalite)	2200	0.6	920	[50]
Mud	2200	1	2000	[50]
Rock (antigorite and clays)	2630	0.5-2.5	2000	[51]
Water	1000	0.56	4200	[49]

7. van Houten-Groeneveld, I. Photoelectric light curve of Pallas. *Astron. Astrophys.* **98**, 203 (1981).

8. Schroll, A., Haupt, H. F. & Maitzen, H. M. Rotation and photometric characteristics of Pallas. *Icarus* **27**, 147–156 (1976).

9. Burchi, R. Some photometric parameters of the minor planet 2 Pallas. *Mem. Societa Astronomica Italiana* **43**, 27 (1972).

10. Lustig, G. & Hahn, G. Photoelektrische Lichtkurven der Planetoiden (2) Pallas und (704) Interamnia. *Acta Phys. Austriaca* **44**, 199–205 (1976).

11. Burchi, R. & Milano, L. 2 Pallas pole revisited. *Moon and Planets* **28**, 17–21 (1983).

12. Vesely, C. D. & Taylor, R. C. Photometric lightcurves of 21 asteroids. *Icarus* **64**, 37–52 (1985).

13. Binzel, R. P. 2 Pallas - 1982 and 1983 lightcurves and a new pole solution. *Icarus* **59**, 456–461 (1984).

14. Carlsson, M. & Lagerkvist, C.-I. Physical studies of asteroids. XI - Photoelectric observations of the asteroids 2, 161, 216 and 276. *Astron. Astrophys. Suppl.* **53**, 157–159 (1983).

15. Burchi, R., D'Ambrosio, V., Tempesti, P. & Lanciano, N. Rotational properties of asteroids 2, 12, 80, 145 and 354 obtained by photoelectric photometry. *Astron. Astrophys. Suppl.* **60**, 9–15 (1985).

16. Lagerkvist, C.-I. & Williams, I. P. Physical studies of asteroids. XV - Determination of slope parameters and absolute magnitudes for 51 asteroids. *Astron. Astrophys. Suppl.* **68**, 295–315 (1987).

17. Lupishko, D. F., Tupieva, F. A., Velichko, F. P. & Bel'Skaya, I. N. Photometry of the asteroids 2, 4, 16, 17, 19, 20, 22 and 505. *Bjull. Inst. Astrofizikii* **80**, 13–17 (1989).

18. Schober, H. J. *et al.* Physical studies of asteroids. XXVIII. Lightcurves and photoelectric photometry of asteroids 2, 14, 51, 105, 181, 238, 258, 369, 377, 416, 487, 626, 679, 1048 and 2183. *Astron. Astrophys.* **105**, 281–300 (1994).

19. Lagerkvist, C.-I., Magnusson, P., Williams, I. P., Buontempo, M. E. & Gibbs, P. Physical studies of asteriods. XVIII - Phase relations and composite lightcurves obtained with the Carlsberg Meridian Circle. *Astron. Astrophys. Suppl.* **73**, 395–405 (1988).

20. Ševeček, P. *et al.* SPH/N-Body simulations of small (D = 10km) asteroidal breakups and improved parametric relations for Monte-Carlo collisional models. *Icarus* **296**, 239–256 (2017).

21. Hilton, J. L. US Naval Observatory Ephemerides of the Largest Asteroids. *Astron. J.* **117**, 1077–1086 (1999).

22. Michalak, G. Determination of asteroid masses — I. (1) Ceres, (2) Pallas and (4) Vesta. *Astron. Astrophys.* **360**, 363–374 (2000).

23. Goffin, E. New determination of the mass of Pallas. *Astron. Astrophys.* **365**, 627–630 (2001).

24. Standish, E. M. Suggested gm values for ceres, pallas, and vesta. Tech. Rep., JPL Interoffice Memorandum (2001).

25. Pitjeva, E. V. Progress in the determination of some astronomical constants from radiometric observations of planets and spacecraft. *Astron. Astrophys.* **371**, 760–765 (2001).

26. Pitjeva, E. V. Estimations of masses of the largest asteroids and the main asteroid belt from ranging to planets, Mars orbiters and landers. In J.-P. Paillé (ed.) *35th COSPAR Sci. Assembly*, vol. 35 of *COSPAR, Plenary Meeting*, 2014 (2004).

27. Pitjeva, E. V. High-Precision Ephemerides of Planets - EPM and Determination of Some Astronomical Constants. *Solar Syst. Res.* **39**, 176–186 (2005).

28. Konopliv, A. S., Yoder, C. F., Standish, E. M., Yuan, D.-N. & Sjogren, W. L. A global solution for the Mars static and seasonal gravity, Mars orientation, Phobos and Deimos masses, and Mars ephemeris. *Icarus* **182**, 23–50 (2006).

29. Baer, J. & Chesley, S. R. Astrometric masses of 21 asteroids, and an integrated asteroid ephemeris. *Celest. Mech. and Dynamical Astron.* **100**, 27–42 (2008).

30. Fienga, A., Manche, H., Laskar, J. & Gastineau, M. INPOP06: a new numerical planetary ephemeris. *Astron. Astrophys.* **477**, 315–327 (2008).

31. Folkner, W. M., Williams, J. G. & Boggs, D. H. The planetary and lunar ephemeris de 421. *IPN Progress Rep.* **42**, 1–34 (2009).

32. Pitjeva, E. V. EPM ephemerides and relativity. In Klioner, S. A., Seidelmann, P. K. & Soffel, M. H. (eds.) *IAU Symposium*, vol. 261 of *IAU Symposium*, 170–178 (2010).

33. Somenzi, L., Fienga, A., Laskar, J. & Kuchynka, P. Determination of asteroid masses from their close encounters with Mars. *Planet. Space Sci.* **58**, 858–863 (2010).

34. Baer, J., Chesley, S. R. & Matson, R. D. Astrometric Masses of 26 Asteroids and Observations on Asteroid Porosity. *Astron. J.* **141**, 143–155 (2011).

35. Konopliv, A. S. *et al.* Mars high resolution gravity fields from MRO, Mars seasonal gravity, and other dynamical parameters. *Icarus* **211**, 401–428 (2011).

36. Zielenbach, W. Mass Determination Studies of 104 Large Asteroids. *Astron. J.* **142**, 120–128 (2011).

37. Fienga, A., Kuchynka, P., Laskar, J., Manche, H. & Gastineau, M. Asteroid mass determinations with INPOP planetary ephemerides. *EPSC-DPS Joint Meeting 2011* 1879 (2011).

38. Fienga, A., Manche, H., Laskar, J., Gastineau, M. & Verma, A. INPOP new release: INPOP10e. *ArXiv e-prints* (2013).

39. Kuchynka, P. & Folkner, W. M. A new approach to determining asteroid masses from planetary range measurements. *Icarus* **222**, 243–253 (2013).

40. Pitjeva, E. V. Updated IAA RAS planetary ephemerides-EPM2011 and their use in scientific research. *Solar Syst. Res.* **47**, 386–402 (2013).

41. Fienga, A., Manche, H., Laskar, J., Gastineau, M. & Verma, A. INPOP new release: INPOP13c. *Sci. Notes* (2014).

42. Goffin, E. Astrometric asteroid masses: a simultaneous determination. *Astron. Astrophys.* **565**, A56 (2014).

43. Viswanathan, V., Fienga, A., Gastineau, M. & Laskar, J. INPOP17a planetary ephemerides. *Notes Sci. et Techniques de l'Institut de mécanique céleste, (ISSN 1621-3823), #108, ISBN 2-910015-79-3 , 2017, 39 pp.* **108** (2017).

44. Baer, J. & Chesley, S. R. Simultaneous Mass Determination for Gravitationally Coupled Asteroids. *Astron. J.* **154**, 76 (2017).

45. Fienga, A. Inpop. *pers. comm.* (2018).

46. Castillo-Rogez, J. C. *et al.* Iapetus' geophysics: Rotation rate, shape, and equatorial ridge. *Icarus* **190**, 179–202 (2007).

47. Durham, W. B., Prieto-Ballesteros, O., Goldsby, D. L. & Kargel, J. S. Rheological and Thermal Properties of Icy Materials. *Space Sci. Rev.* **153**, 273–298 (2010).

48. Grimm, R. & McSween, H. Water and the thermal evolution of carbonaceous chondrite parent bodies. *Icarus* **82**, 244–280 (1989).

49. Waite, W. F., Stern, L. A., Kirby, S. H., Winters, W. J. & Mason, D. H. Simultaneous determination of thermal conductivity, thermal diffusivity and specific heat in sI methane hydrate. *Geophys. J. Int.* **169**, 767–774 (2007).

50. Schofield, N. *et al.* Mobilizing salt: Magma-salt interactions. *Geology* **42**, 599–602 (2014).

51. Grindrod, P. M. *et al.* The long-term stability of a possible aqueous ammonium sulfate ocean inside Titan. *Icarus* **197**, 137–151 (2008).